Int J Ind Chem (2015) 6:261–271
DOI 10.1007/s40090-015-0047-7

RESEARCH

One-pot sonochemical synthesis of CdS nanoparticles: photocatalytic and electrical properties

Dasari Ayodhya[1] · M. Venkatesham[1] · A. Santoshi kumari[1] · G. Bhagavanth Reddy[1] · G. Veerabhadram[1]

Received: 12 March 2015 / Accepted: 4 July 2015 / Published online: 24 July 2015

Abstract CdS nanoparticles (NPs) are synthesized by sonochemical method using tryptophan as a capping agent. The synthesis process is of one step, using biocompatible capping agent, which is nontoxic. The synthesized NPs are characterized by UV–Vis absorption, fluorescence, FTIR, XRD, TGA, DLS, SEM and TEM. The size of NPs is below 10 nm, as observed from XRD and TEM characterizations. Photocatalytic degradation of methyl orange (MO) dye by the CdS NPs as photocatalysts under sunlight irradiation has been studied. The kinetics of catalysis of synthesized CdS NPs with MO dye follows pseudo-first-order kinetics with reasonable apparent rate constants. A variation of dielectric constant as a function of frequencies of an alternating electric field has been observed with the prepared tryptophan-capped CdS NPs deposited at different concentrations. The electric conductivity of CdS NPs is found to increases with the concentration of tryptophan.

Keywords CdS nanoparticles · Photodegradation · Kinetic study · Dielectric constant · DC conductivity

Introduction

Among the II–VI semiconductors, CdS is one of the first semiconductors to be discovered and is probably one of the most important electronic and optoelectronic materials, with prominent applications in nonlinear optical devices, flat panel displays, light emitting diodes, lasers, logic gates, transistors, etc [1–3]. Many studies have focused on CdS because of its high photosensitivity and potential application in photoconducting cells and a variety of optoelectronic conversion devices including photodetectors and thin film solar cells [4]. A large number of synthetic methods such as solvothermal, hydrothermal [5, 6] and sonochemical process [7], microwave heating [8] and solution-based chemical methods [9] provide effective routes to prepare semiconductor nanoparticles. For nanoparticles prepared by solution-based chemical methods, a capping agent, which adsorbs on to the nanoparticle surface, is generally added both to control the size of the nanoparticles and to prevent agglomeration of the synthesized particles. These adsorbents have been shown to alter the electronic structure of the nanoparticles [10, 11].

Synthesis of CdS nanoparticles in large scale is important for industrial applications in the areas of catalysis, photocatalysis and microelectronics [12]. CdS NPs have two common crystalline phases of hexagonal wurtzite and cubic zinc blende [13–15]. The bulk wurtzite structure is a thermodynamically stable phase which exists under normal conditions (such as atmospheric pressure and room temperature) [16]. The difference in intrinsic energy between these two phases is minor. It was considered that the phase stability between the zinc blende and wurtzite structures of CdS was size dependent. Generally, the cubic CdS nanoparticles exist in smaller sizes and in the wurtzite structure appear larger due to the growth of the particles [17–19].

Currently, the sonochemical method has been used extensively to generate novel materials with unusual properties, since they form particles of a much smaller size and higher surface area than those reported by other methods [20]. Ultrasound irradiation offers a very attractive method for the preparation of nanosized materials and

✉ G. Veerabhadram
gvbhadram@gmail.com

[1] Department of Chemistry, Osmania University, Hyderabad 500007, India

has shown very rapid growth in its application to materials science, due to its unique reaction effects. It is well known that many properties of CdS NPs, such as crystalline phase, size, morphology, specific surface area and defects, can affect its photocatalytic activity [21]. It has been suggested that the specific surface structure of photocatalyst could be effective in the suppression of recombination between photo-generated electrons and holes. A semiconductor photocatalyst with high activity should have high crystalline and large specific surface area. The photocatalytic activity of CdS is mainly dependent on the electrons and holes which are produced by light absorption [22]. Photocatalysis is a potential technology for the destruction of organic contaminants in water, such as aromatic compounds which present a potential hazard to the environment. Photocatalytic process is a photoreaction with a catalyst and depends on the nature of the catalyst because of its ability to create electron–hole pairs, which generate free radicals having the ability to undergo secondary reactions [23]. Sudheer khan et al. [24] reported the synthesis of CdS NPs with photocatalytic activity under visible light. The particle with photo-activity under visible light has wide application in textile and food-processing industries. In general, for nanomaterials, the grain boundaries play an important role in the electric and dielectric properties. The electrical conductivity and dielectric behavior of nanocrystalline materials depend on chemical compositions, preparation conditions and particle size.

Tryptophan is an essential amino acid, necessary for the production of several critical substances in the body (e.g., serotonin), as well as in the human diet. Moreover, using tryptophan as capping agent will not induce any environmental toxicity in the CdS NPs formation process. The interaction of tryptophan with NPs occurs via the unshared electron pair on the nitrogen atom and is a result of the formation of a complex between the metal and the π-electrons of the indole ring of tryptophan. The indole ring of tryptophan can participate in π–π stacking interactions for nanoparticle self-assembly and is a fluorescent amino acid that could serve as a probe in non-biological environments. The growth of the particle decreases in the presence of tryptophan, a capping agent. Two effects are considered to explain the decrease in particle size in the presence of a capping agent. First, the growth of the particles may be considered as a polymerization reaction with the capping molecule playing the role of a terminator of the chain. Second, as the precipitation is often not complete, because of the capping of Cd^{2+} ions by carboxylic acid (–COOH) and amine ($–NH_2$) groups of tryptophan, smaller particles may simply result. It is found that the particle size decreases in the presence of a capping agent due to restriction of growth of particles.

The aim of this work is to synthesize CdS NPs with different concentrations of tryptophan by a novel and simple method. The samples were characterized using TEM, SEM, XRD, FTIR, TGA, fluorescence and UV–visible spectroscopy for the structural, thermal and optical behavior of the CdS NPs. The photocatalytic degradation of MO dye was carried out in the presence of CdS NPs under sunlight irradiation. The kinetic rate constant of degradation is higher in the presence of low concentration of tryptophan-capped CdS NPs than in high concentrations. To find the changes in the electrical properties of CdS NPs, an extensive study was done to investigate the dielectric properties and DC conductivity of the samples.

Experimental

Synthesis of CdS NPs

CdS NPs were synthesized by the sonochemical method using a sonochemical bath at room temperature. The procedure for the preparation of CdS NPs is as follows. 0.1 M cadmium acetate was mixed with 0.1 M sodium sulfide and an equal amount of tryptophan was used as the chelating agent. The chelating agent concentration plays an important role in controlling the size of NPs. After mixing all the three constituents in the conical flask, it was kept in a sonochemical bath (ultrasonic power 50 Watts, model no. 1.5L 50H, Biotechnics, India) at room temperature. Different concentrations of tryptophan, viz., (a) 0.1 M, (b) 0.2 M and (c) 0.3 M were used. Then the individual solutions were exposed to ultrasound irradiation for 60 min. After the irradiation, the yellow color suspension that formed was centrifuged to get the precipitate out and washed several times with double-distilled water and ethanol to remove the unreacted reagents. Finally, the product was dried in an oven at 80 °C for 6 h and analyzed further.

Characterization techniques

The UV–visible absorption spectra of CdS NPs were recorded using a Shimadzu UV-3600 series spectrophotometer in the spectral range of 200–800 nm. The fluorescence spectrum was measured with an RF-5301PC spectrofluorophotometer (Shimadzu, Japan). X-ray diffraction (XRD) pattern was recorded on X'Pert PHILIPS, 30 kV, 40 mA with Ni-filter CuKα radiations. FTIR (Fourier transform infrared) spectra on KBr pellet were recorded on a Shimadzu spectrophotometer in the range of 4000 to 400 cm^{-1}. Transmission electron microscopy (TEM) and scanning electron microscopy (SEM)

photographs were obtained on a TechnaiG2 microscope operated at 200 kV and ZEISS EVO18 electron microscope. The TGA (thermogravimetric analysis) studies were performed in DTG-60H instrument (Shimadzu, Japan). DLS (dynamic light scattering) measurements were determined with the Zetasizer Nano ZS (Malvern Instruments, UK). Electric conductivity, dielectric and impedance measurements were carried out on a Klaynekerr LCR-6440B impedance analyzer from 200 Hz to 1 MHz.

Photocatalytic degradation of methyl orange dye

Methyl orange dye (sodium 4-[(4-dimethylamino) phenyldiazenyl] benzenesulfonate, $C_{14}H_{14}N_3NaO_3S$) is a very stable azo dye and has been used as a probe for photocatalytic decolorization [25, 26]. MO is commonly considered as a representative organic dye in textile effluents, which can be easily monitored by optical absorption spectroscopy. The UV–visible spectra of the MO solution show two major absorption peaks at 270 and 462 nm in the initial spectra, which are due to the benzene ring and azo linkage [27].

The photocatalytic activities of the CdS NPs at different concentrations were carried out in a glass reactor of 100 ml capacity for degrading MO in water solution. In a typical photocatalytic test, 20 mg of CdS NPs was loaded in a RB flask containing 60 ml of 5×10^{-6} M concentration of dye solution under sunlight irradiation. Prior to the start of the irradiation, dark adsorption was carried out for 1 h under continuous stirring to establish equilibrium between the dye and the catalyst. The dye concentration was monitored at regular time intervals by measuring the maximum UV absorbance of MO at 462 nm by UV–visible spectrophotometer.

Dielectric constant measurement

The dielectric properties of CdS NPs were studied in the frequency range of 200 Hz–1 MHz at room temperature. The dielectric constant was evaluated using the relation

$$\varepsilon = \frac{Cd}{\mathrm{A}\ \varepsilon_0},$$

where ε_0 is the vacuum permittivity, d is the thickness and A is the area of the sample. The capacitance and conductance of all the samples were measured with the impedance analyzer. These were used to evaluate the real (Z') and imaginary (Z'') parts of the complex impedance. The DC conductance was determined from the semicircular complex impedance plots (Z' versus Z'') by taking the value of the intersection of the low-frequency end of the semicircular on the Z' axis. The conductivity of each sample was calculated using the expression:

$$\sigma = \frac{d}{A \times R},$$

where R is the resistance, d and A are the thickness in cm and cross-sectional area in cm^2 of the samples.

Results and discussion

UV–visible absorption analysis

The influence of the concentration of tryptophan on the CdS NPs size was studied by recording the absorption spectra. From Fig. 1, it is clear that there is a slight blue shift in the absorption edge of the CdS NPs when the concentration of tryptophan in the preparation changed from 0.3 to 0.1 M. The absorption spectra observed here for these particles are the same as those in the literature [28, 29]. The band gap, determined for the present investigation and found to be 2.62–2.51 eV. Compared with the band gap of bulk CdS, it reveals an enhancement of optical band gap from 2.42 eV. This clearly indicates the nanophase and quantized nature of the prepared CdS NPs. However, in the present case, the observation of band gaps probably implies that the sample consists of distinct particles, with slightly smaller ones showing a cubic structure. As the particle size gets smaller, the energy levels move farther apart and become more discrete. The results also reveal that the band gap increases with the decrease of particle size due to the quantum size effects. The band gap energy of NPs is dependent on particle size and lattice structure; to understand the transitions between the electronic states requires a quantum theory treatment. From the position of the absorption edge, the average particle size can be determined using Henglein's empirical relation between particle size and the absorption wavelength [30, 31].

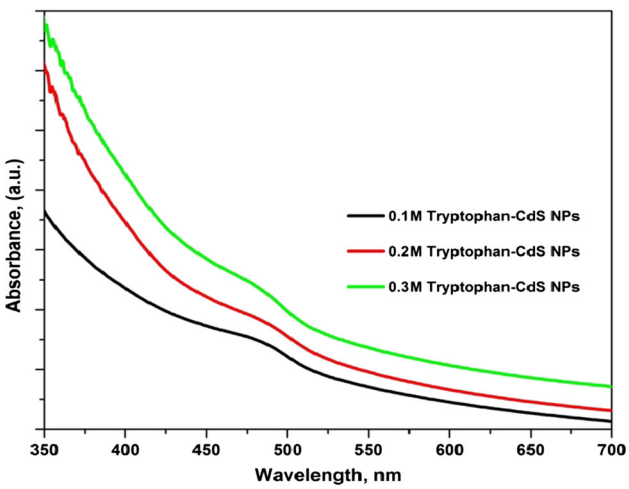

Fig. 1 UV–visible absorption spectra of tryptophan-capped CdS NPs

Fluorescence analysis

The photoluminescence (PL) property is influenced by the structure, composition, particle size and morphology of the CdS NPs. Figure 2 shows the PL spectrum of CdS NPs, excited with wavelength 350 nm. It shows the broad emission bands around 448, 466 and 473 nm for 0.1, 0.2 and 0.3 M tryptophan-capped CdS NPs, respectively. The observed PL peaks are markedly blue shifted relative to that of the bulk CdS (~500 nm). This shift in the PL emission further provides evidence in support of quantum effects in the nanoparticles. The observation of PL spectra depends very much on the size distribution of nanoparticles. If the distribution is very broad, a large number of particles of different sizes will always be excited. This is probably due to the difference in the sizes of CdS NPs. It is evident from the PL spectra that the corresponding broad emission band for the sample can be assigned to the surface trap-induced fluorescence which involved the recombination of electrons trapped inside a sulfur vacancy with the hole in the valence band of CdS NP. From the PL spectra, the position of the emission peak shifts toward higher energy with the decrease of NPs size.

FTIR spectroscopic analysis

The FTIR spectra of pure tryptophan and different concentrations of tryptophan-capped CdS NPs are shown in the range of 4000 to 400 cm^{-1} in Fig. 3. In the FTIR spectrum of pure tryptophan, the strong absorption peaks at 3402, 3037, 2561, 1589, 1411, 1357, 1059 and 744 cm^{-1} are assigned to N–H stretching in amines, C–H stretching in alkenes, O–H stretching in carboxylic acids, N–H bending in amines, C–H bending in alkanes, C–N stretching in aryl amines and C–H bending in aromatic ring, respectively. For the tryptophan-capped CdS NPs, when compared with pure tryptophan, the decrease in the intensity is followed by the increase in broadness of the peaks in all the cases at 3433, 1638, 1560 and 1411 cm^{-1}. The absorption band is weak at 742 cm^{-1}, and disappearance of a peak at 3037 cm^{-1} suggests that N–H stretching is absent. These observations led us to conclude that the indole ring did not interact with the CdS NPs surface, while both amino and carboxy groups of tryptophan were the preferential terminal groups to attach onto the surface of CdS NPs. As the main part of the tryptophan molecule is formed of an indole group and the indole group contains a nitrogen atom, it is likely to consider that these primary amine groups are involved in the complexation of the amino acid with the CdS surface. This clearly indicates that the tryptophan molecules cap and stabilize the CdS NPs.

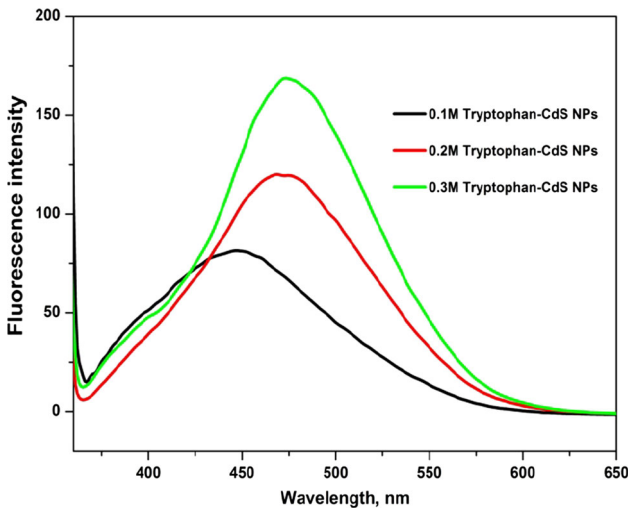

Fig. 2 Fluorescence emission spectra of tryptophan-capped CdS NPs

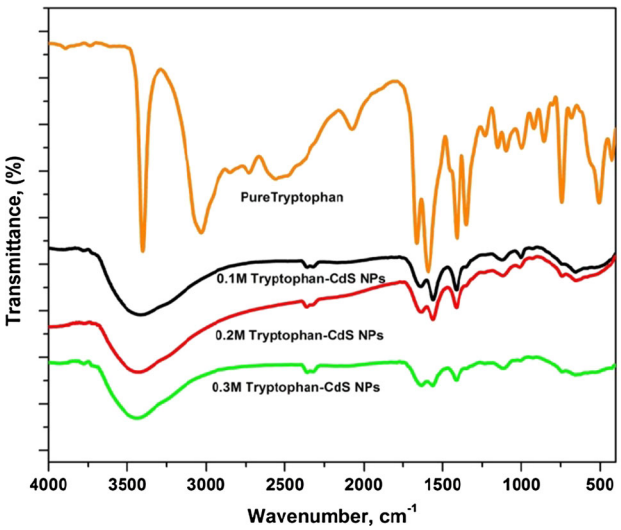

Fig. 3 FTIR spectrum of pure tryptophan and tryptophan-capped CdS NPs

X-ray diffraction analysis

X-ray diffraction pattern gives information about the crystalline structure and crystal size. Figure 4 shows the X-ray diffraction pattern of the CdS NPs capped with tryptophan of different concentrations. XRD peaks are found to be at 2Θ values of 26.2 ± 0.2, 43.3 ± 0.2 and 51.6 ± 0.2 corresponding to the (111), (220) and (311) crystal planes, respectively. The XRD pattern reveals the existence of both cubic and hexagonal phases. The cubic phase is dominant by its strong peaks of (111), (220) and (311) and the relatively weak peak of (101) which appeared at 2Θ values of 30 ± 0.8. The broadened of diffraction peak provides information about the sizes of the particles being in the nano range. As the width increases, the particle

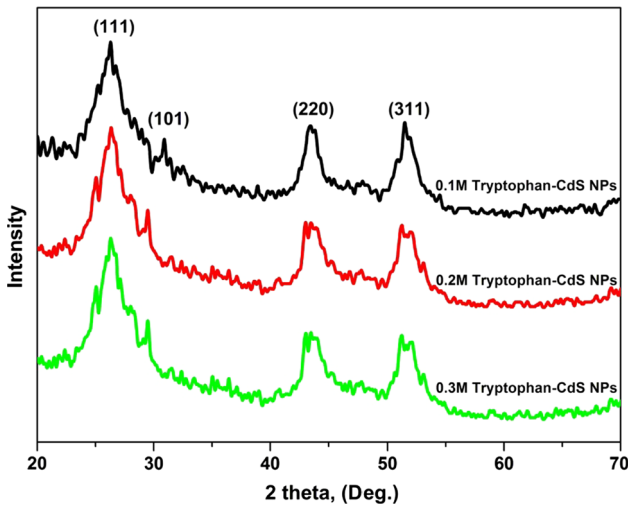

Fig. 4 XRD patterns of tryptophan-capped CdS NPs

size decreases and vice versa [32]. The average crystal size is calculated from Scherrer formula [33]. The average crystal size of the samples lies in the order of 6.2 ± 2.1 nm. The lattice constant (*a*) was calculated to be 5.8 Å for these samples, which matches with the earlier reported lattice constant for cubic zinc blend structure of CdS NPs [34].

Scanning electron microscopy analysis

Figure 5a, b presents the typical SEM photographs and EDAX of CdS NPs, respectively. Obviously, many small particles had covered up the whole surface area and embedded in the cross-sectional area of CdS NPs. The composition of the product was studied and it was proved that the elements were Cd and S with an atom ratio of 1:1 by EDAX (energy-dispersive analysis X-ray). The chemical composition of CdS NPs was measured through the EDAX spectrum. According to EDAX, the particles consist of C, O, Cd and S. The peaks of C and O were mainly generated by tryptophan and the peaks of Cd and S were generated by CdS NPs. The elemental weight percentage of C, O, Cd and S are 19.87, 19.13, 32.02 and 28.24, respectively, and are present in tryptophan-capped CdS NPs.

Transmission electron microscopy analysis

The typical TEM images, particle size distribution and corresponding SAED image for the tryptophan-capped CdS NPs are shown in Fig. 6a–d, respectively. It is observed that CdS NPs can change from the dispersion to the aggregation state. This indicates the interaction between tryptophan and the CdS NPs. The NPs showed similar shapes and different sizes. Although the NPs average mean

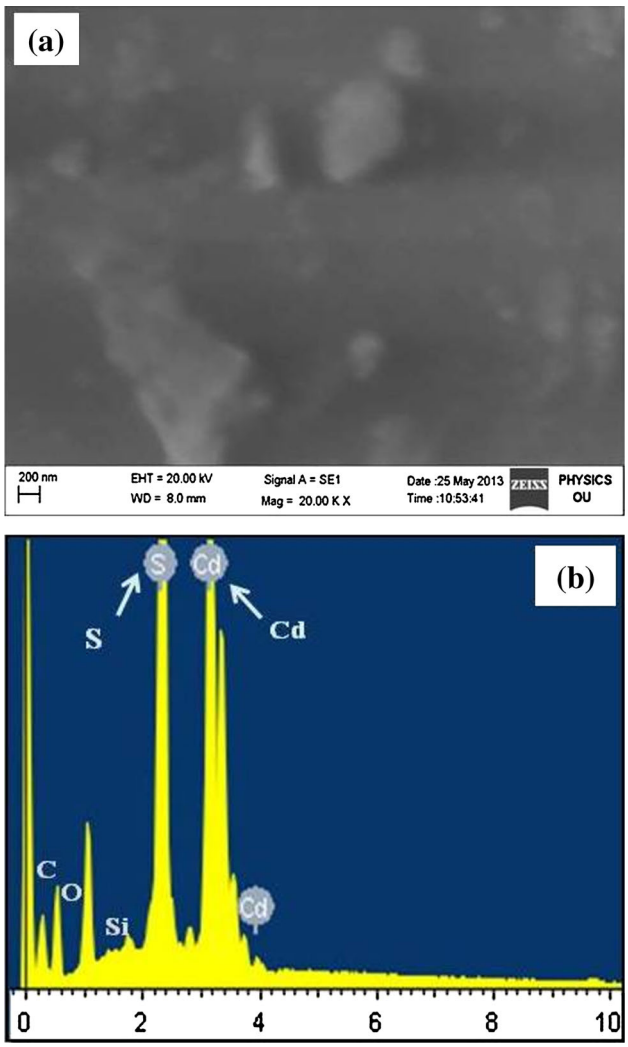

Fig. 5 **a** High-resolution SEM image and **b** EDAX spectra of CdS NPs

size is 6 nm for the solutions with isolated particles, the particles agglomerate together to release a large surface energy, but can be dispersed by ultrasonic oscillation or vigorous stirring.

Thermogravimetric analysis

The thermal behavior of the prepared CdS NPs has been studied by TG–DTA. Since temperature plays an important role in the formation of nanostructured materials, temperature-induced phase changes are significant for the utility of these NPs for various applications. The TGA of CdS NPs at different concentrations of tryptophan was attempted up to a temperature of 800 °C under a nitrogen atmosphere. In Fig. 7, the thermogram of CdS NPs shows that the mass loss began at 115–202 °C. Weight loss at about 202 °C corresponds to the adsorbed water on the surface of

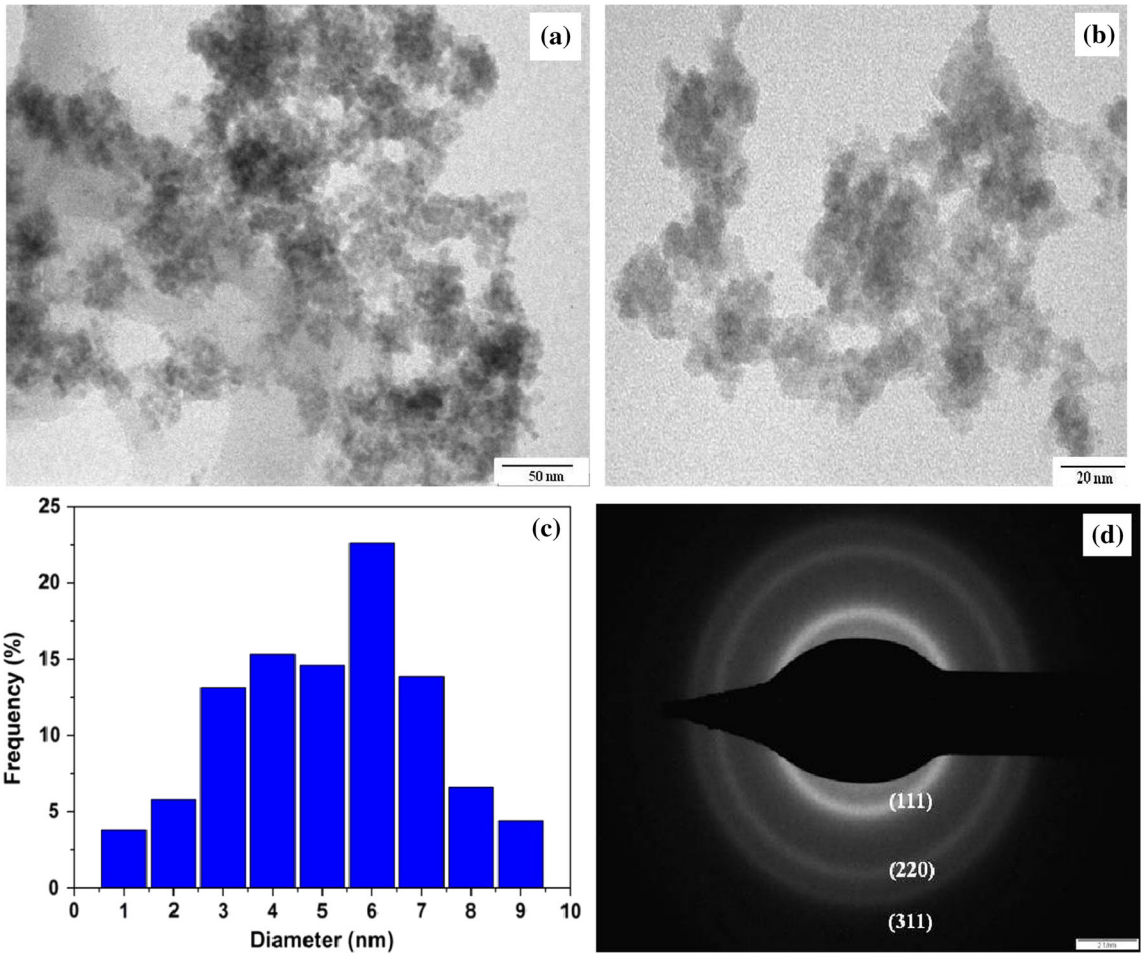

Fig. 6 **a**, **b** TEM images, **c** particle size distribution and **d** SAED of CdS NPs

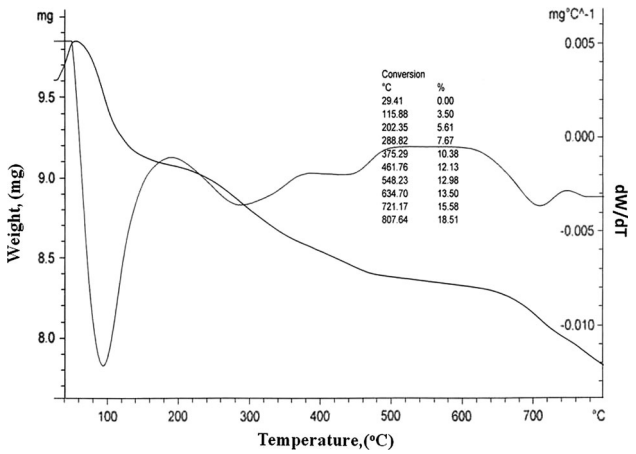

Fig. 7 TG–DTA of the 0.1 M tryptophan-capped CdS NPs

NPs. Similarly, it shows the second stage of degradation between 202 and 461 °C, which indicates clearly a change in the nature of binding of the oxidized tryptophan molecules coordinated to the CdS NPs surface in the spontaneously reduced sample. Above 461 °C, CdS NPs degradation takes place slowly up to 800 °C. The percentage of weight loss for 0.1, 0.2 and 0.3 tryptophan-capped CdS NPs is 18.51, 18.80 and 27.54 % respectively.

Dynamic and electrophoretic light scattering analysis

Zeta potential is a crucial parameter for stability in aqueous nanosuspensions. For a physically stable nanosuspension solely stabilized by electrostatic repulsion, a zeta potential of ±30 mV is required as a minimum [35]. Zeta potentials of tryptophan-capped CdS NPs are shown in Fig. 8a. Electrophoretic light scattering was used to determine the zeta potential of the dispersed NPs. Electrophoresis indicated that the zeta potential of the particles was −40.1 mV. The particles demonstrate a strong negative zeta potential, due to the carboxylate groups on the surface, and exhibit excellent colloidal stability.

DLS is a commonly used particle sizing method that can be carried out directly in aqueous solution. DLS has been applied to a number of systems, including both organic and

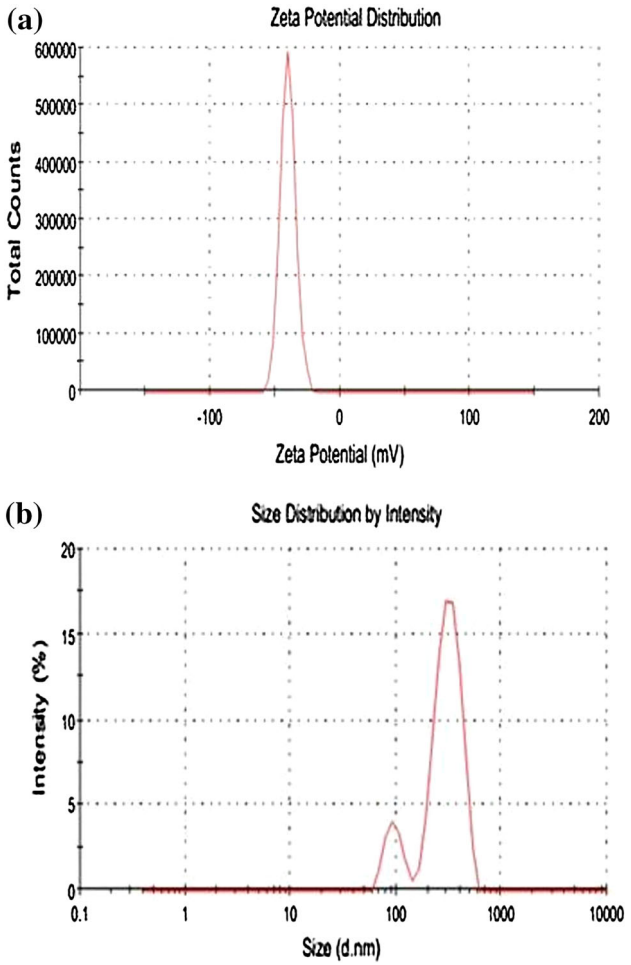

Fig. 8 **a** Zeta potential and **b** size distribution of tryptophan-capped CdS NPs

inorganic nanoparticles and for species ranging in size from nanometers to microns [36]. However, because the diameters measured by DLS are hydrodynamic, the results can be affected by the attributes of the system other than the primary nanoparticle size, such as the aggregation state [37]. The sizes of CdS NPs measured by DLS were highly dependent on the concentration of the solution in which the nanoparticles were prepared. The diameter deviates at higher concentration from that determined by TEM. This disagreement between diameters measured by DLS and TEM at high concentration is due to the electrostatic repulsion between nanoparticles being diminished at high concentration, resulting in the formation of aggregates of CdS NPs. Because aggregates of nanoparticles will diffuse more slowly in solution than individual nanoparticles, the aggregates effectively behave as larger particles. Therefore, the hydrodynamic diameter determined by DLS will not reflect the primary nanoparticle size, but rather that of the aggregate. The results of DLS, shown in Fig. 8b, demonstrate the size distribution of the CdS NPs.

Photocatalytic activity

The performance of the photocatalytic activity of MO dye in the presence and absence of CdS NPs was studied under sunlight. During sunlight irradiation in the absence of CdS NPs, no variation in absorbance was found. But in the presence of CdS NPs, it was observed that the absorbance at 462 nm decreased. Both the decrease in intensity and hypsochromic shifts of absorption peaks are also meaningful with respect to the −N=N− of MO. Especially, after sunlight irradiation for 4 h, these two peaks of MO solution almost totally disappear, indicating that the benzene ring and azo linkage of MO are destroyed by CdS NPs. The results indicate that the prepared CdS NPs can be used as a suitable and promising photocatalyst for effective decolorization treatment of dye-containing effluents. Figure 9 shows the degradation efficiency of MO dye in the absence and presence of a catalyst. It is observed that in the absence of a catalyst, the degradation efficiency was only 18.55 % in 4 h. To improve the efficiency, CdS NPs was added into the MO solution. When the different concentrations of CdS NPs such as 0.1, 0.2 and 0.3 are used, the degradation efficiency is found to be 75.33, 73.92 and 70.33 %, respectively. Especially, we found that the color of the MO solution under the as-synthesized CdS photocatalysis had almost changed from orange to white after 4 h illumination of sunlight, which revealed that the synthesized CdS NPs could degrade the MO solution effectively and have stronger photocatalytic degradation ability than the reported CdS, CdS/TiO_2 systems [38–41]. The enhancement could be explained on the basis that as the concentration of tryptophan decreases, the particles size also decreases as well as surface area increases and then the photocatalytic activity increases.

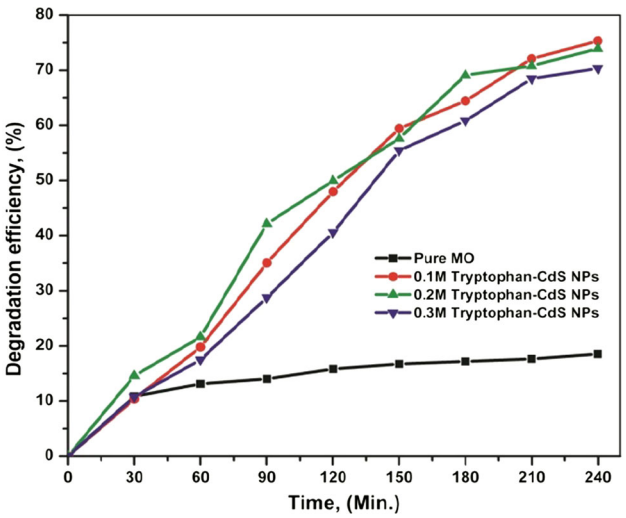

Fig. 9 The degradation of MO dye in the absence and presence of CdS NPs under sunlight irradiation

Determination of kinetic rate constants

The kinetics of MO photodegradation catalyzed by synthesized CdS NPs was studied under sunlight. The photocatalytic degradation of various organic compounds such as dyes in the presence of a heterogeneous photocatalyst can be formally described by the Langmuir–Hinshelwood kinetics model [42]:

$$\text{Rate } (r) = \mathrm{dC/dt} = k\ \mathrm{KC}/1 + \mathrm{KC}.$$

For low concentrations of dyes, KC$\ll$1, neglecting KC in the denominator and integrating with respect to time t, the above equation can be simplified to the pseudo-first-order kinetic model equation:

ln $C_o/C_t = k\ Kt = K_{app}\ t$; then the equation is modified as ln $A_o/A_t = K_{app}\ t$, where dC/dt is the rate of dye degradation (mg L^{-1} min^{-1}), k is the reaction rate constant (min^{-1}), K is the adsorption coefficient of the dye on to the photocatalyst particle (L mg^{-1}) and K_{app} (min^{-1}) is the apparent rate constant calculated from the curves. The apparent rate constants of degradation of MO dye with CdS NPs, K_{app}, were determined from the slopes of the plots and are in accordance with the proposed pseudo-first-order kinetic model as shown in Fig. 10. The apparent rate constants and degradation efficiencies are given in Table 1, which show that the photodegradation of the MO dye decreases from 0.1 to 0.3 M tryptophan-capped CdS NPs.

Dielectric analysis

Figure 11 shows the plot of the dielectric constant versus applied frequency of CdS NPs in the frequency range of 200 Hz–1 MHz at room temperature. It is observed that the dielectric constant decreases exponentially with increasing frequency and then attains almost a constant value in the high-frequency region. The high value of the dielectric constant at low frequencies may be due to the presence of all the four polarizations, namely, space charge, orientation, electronic and ionic polarizations. Its low value at higher frequencies may be due to the gradual loss of significance of these polarizations [43]. This may lead to large values of dielectric constant at low frequencies. The dielectric constant values of the CdS NPs is found to be very high compared to that of the bulk CdS, which is in good agreement with the earlier reports [44]. As the particle size is in nanometer order, the number of particles per unit volume is large; hence, the dipole moment per unit volume increases as the dielectric constant increases. In this case, two possible reasons can be considered. The first one is that in the presence of CdS NPs, the conductivity of the sample increases. The second one is the influence of the existence of small particles which can affect the energy shift in the band structure of the sample. The result of this process affects the conductivity of the samples.

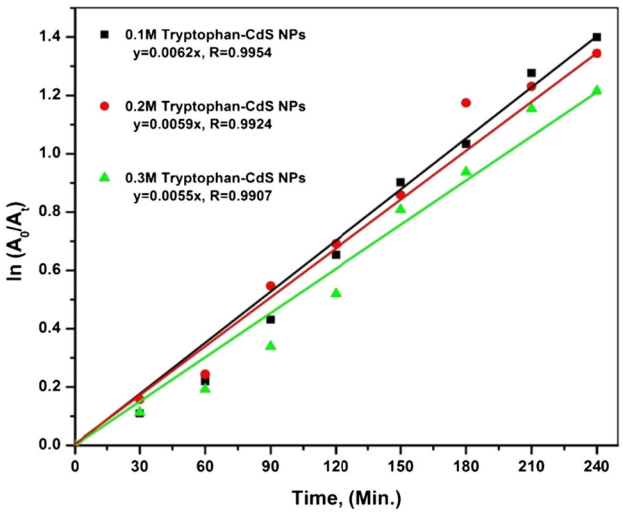

Fig. 10 Observed apparent rate constants of photodegradation of MO in the presence of CdS NPs

Table 1 The values of percentage of degradation and rate constants of CdS NPs for various concentrations of tryptophan-capped CdS NPs

S.no	Sample	Degradation efficiency (%)	Rate constants (k, min^{-1})
1	0.1 M Tryptophan-CdS NPs	75.33	0.0062
2	0.2 M Tryptophan-CdS NPs	73.92	0.0059
3	0.3 M Tryptophan-CdS NPs	70.33	0.0055

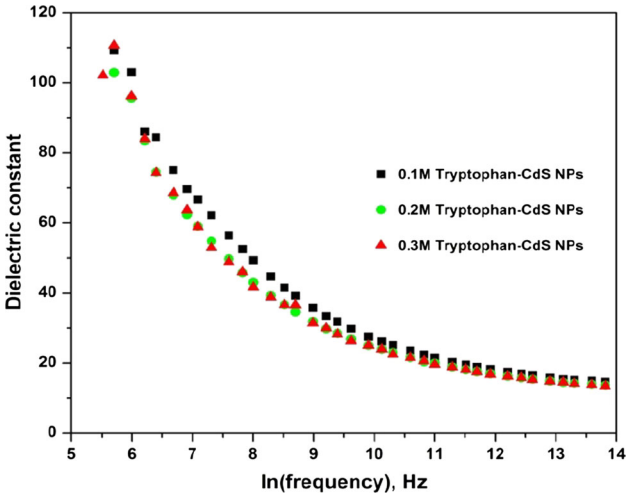

Fig. 11 Variation of dielectric constant of CdS NPs with frequency

DC conductivity study

Figure 12 shows the variation of the (a) real part of impedance (Z') and the (b) imaginary part of impedance (Z'') as a function of frequency on log–log scale at room

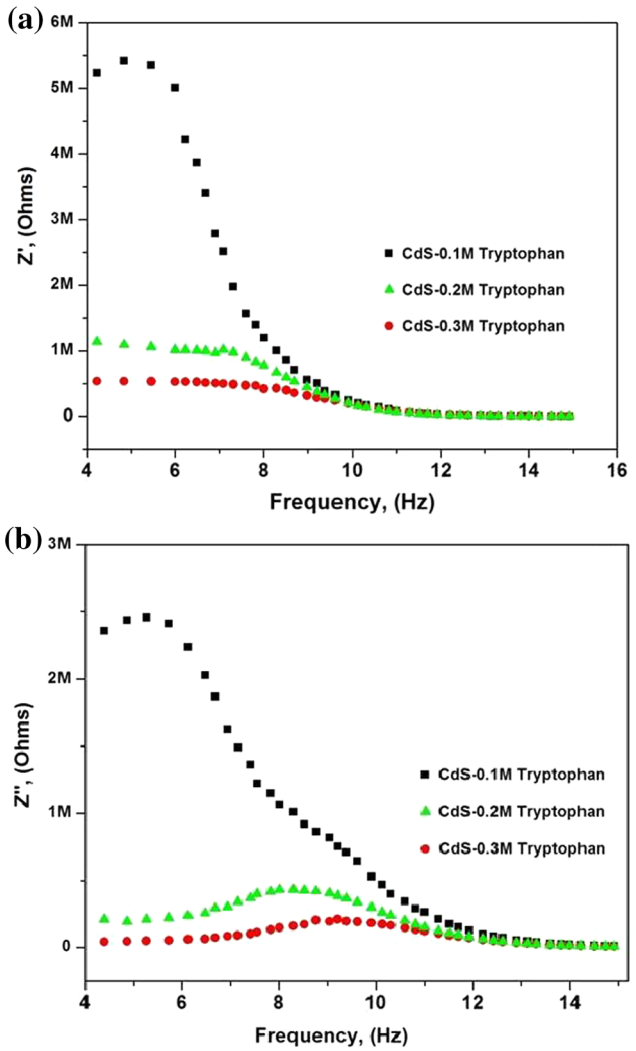

Fig. 12 **a** Variation of real part of impedance (Z′) and **b** imaginary part of impedance (Z″) of CdS NPs as a function of frequency

temperature. The Z', Z'' values of CdS NPs increased with increase of frequency and attained a peak at a particular frequency and then decreased. The frequency at which the peak is attained depends on the concentration of the measurement. The peak frequency is larger at lower concentration.

The values of Z' and Z'' plotted on the complex plane take the form of semicircles, known as Cole–Cole plots [45]. These plots are almost perfect semi-circles. It is known that the observation of semicircle in the $Z''-Z'$ plots indicates the presence of single relaxation species [46]. In Fig. 13, the Z'' is plotted against Z' (Cole–Cole plots) of CdS NPs at room temperature. It clearly indicates that the impedance decreases with the increase of tryptophan concentration. All samples have a semicircle arc starting at the origin point. This indicates that each sample can be described by one bulk resistance and one bulk capacitance and both are connected parallel. The center below the real

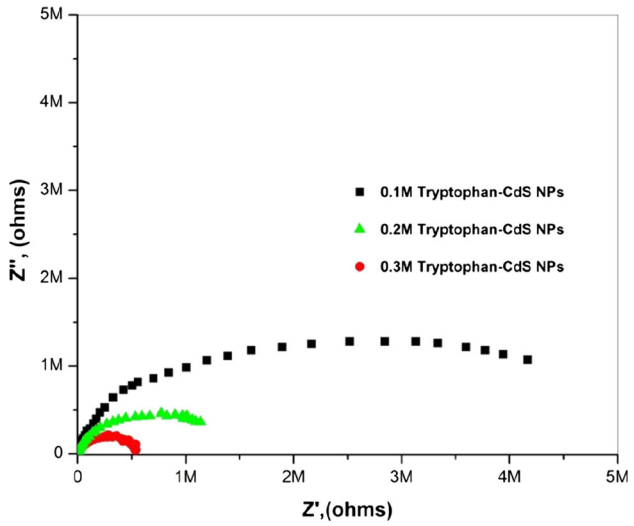

Fig. 13 Cole–Cole plot of CdS NPs

axis (Z') indicates the relaxation behavior of the system. The intercept of the semicircles on the real axis gives the resistance of the corresponding component, contributing toward the impedance of the samples. The DC conductivities determined from impedance plots from the intercepts on the real axis (Z') correspond to zero frequency. The intercept point shifted to lower and lower Z' values with increase of tryptophan concentration. The values of DC conductivities are 0.3474×10^{-7}, 0.9898×10^{-7} and 2.05×10^{-7} S cm^{-1} of 0.1, 0.2 and 0.3 M tryptophan-capped CdS NPs, respectively.

Conclusions

In this paper, we report on sonochemically synthesized CdS NPs capped by tryptophan. Capping of CdS NPs by tryptophan imparts biocompatibility and makes it amenable to biological manipulations. Besides providing stability to the particles against aggregation, the tryptophan cap on the surface effectively passivates the electronic defects on the CdS surface, thereby enhancing the luminescence. In the absorption spectra, as the tryptophan concentration increased, a blue shift was observed. From the SEM, TEM and XRD analyses, the morphology was found to be with cubic zinc blende structure and particle size of <10 nm. TGA was recorded to study the thermal behavior up to 800 °C of the prepared CdS NPs. The CdS NPs exhibit excellent photocatalytic activity for the degradation of MO under sunlight irradiation. The dielectric properties of CdS NPs are found to be significantly enhanced, especially in the low-frequency region due to confinement. The DC conductivity measurements reveal that the conduction depends on both the frequency and concentration of the sample.

Acknowledgments The authors would like to acknowledge DMRL (Defence Metallurgical Research Laboratory), Hyderabad, for providing the necessary facilities. One of the authors, D. Ayodhya, wishes to thank the University Grants Commission, New Delhi, for the award of Junior Research Fellowship.

References

1. Pan H, Poh CK, Zhu YW, Xing GC, Chin KC, Feng YP, Lin JY, Sow CH, Ji W, Wee ATS (2008) Novel CdS nanostructures: synthesis and field emission. J Phys Chem C 112:11227–11230. doi:10.1021/jp8023843
2. Lin YF, Song JH, Ding Y, Lu SY, Wang ZL (2008) Alternating the output of a CdS nanowire nanogenerator by a white-light-stimulated optoelectronic effect. Adv Mater 20:3127–3130. doi:10.1002/adma.200703236
3. Shen GZ, Cho JH, Yoo JK, Yi GC, Lee CJ (2005) Synthesis of single-crystal CdS microbelts using a modified thermal evaporation method and their photoluminescence. J Phys Chem B 109:9294–9298. doi:10.1021/jp044888f
4. Stanely AG (1975) Cadmium sulfide solar cells. In: Advances in materials and device research. Academic, New York, Appl Solid State Sci 5:251–366
5. Zhou M, Yan S, Shi Y, Yang M, Sun H, Wang J, Yin Y, Gao F (2013) Surface-roughness-assisted formation of large-scale vertically aligned CdS nanorod arrays via solvothermal method. Appl Surf Sci 273:89–93. doi:10.1016/j.apsusc.2013.01.191
6. Cao Y, Hu P, Jia D (2013) Phase- and shape-controlled hydrothermal synthesis of CdS nanoparticles, and oriented attachment growth of its hierarchical architectures. Appl Surf Sci 265:771–777. doi:10.1016/j.apsusc.2012.11.107
7. Lopes PAL, Santos MB, Mascarenhas AJS, Silva LA (2014) Synthesis of CdS nano-spheres by a simple and fast sonochemical method at room temperature. Mater Lett 136:111–113. doi:10.1016/j.matlet.2014.07.173
8. Wada Y, Kuramoto H, Anand J, Kitamura T, Sakata T, Mori H, Yanagida SJ (2001) Microwave-assisted size control of CdS nanocrystallites. Mater Chem 11:1936–1940. doi:10.1039/b101358k
9. Bandaranayake RJ, Wen GW, Lin JY, Jiang HX, Sorensen CM (1995) Structural phase behavior in II–VI semiconductor nanoparticles. Appl Phys Lett 67:831–833. doi:10.1063/1.115458
10. Seker F, Meeker K, Kuech TF, Ellis AB (2000) Surface chemistry of prototypical bulk II–VI and III–V semiconductors and implications for chemical sensing. Chem Rev 100:2505–2536. doi:10.1021/cr980093r
11. El-Sayed MA (2004) Small is different: shape-, size-, and composition-dependent properties of some colloidal semiconductor nanocrystals. Acc Chem Res 37:326–333. doi:10.1021/ar020204f
12. Prabhu RR, Khadar MA (2005) Characterization of chemically synthesized CdS nanoparticles. J Phys 65:801–807
13. Morales RL, Angel OZ, Sandoval SJ, Delgado GT (2002) Extra Raman modes in CdS during cubic to hexagonal structural transformation. J Raman Spectrosc 33:460–465
14. Filatova EO, Andre JM, Taracheva EY, Tvaladze AJ, Kraizman VL, Novakovich AA, Vedrinskii RV (2004) Experimental and theoretical studies of orientational dependence of x-ray reflectivity in vicinity of S K-edge in hexagonal CdS crystal. J Phys Condens Matter 16:4597–4606
15. Wright K, Gale JD (2004) Inter atomic potentials for the simulation of the zinc blende and wurtzite forms of ZnS and CdS: bulk structure, properties, and phase stability. Phys Rev B 70:035211/1–035211/8. doi:10.1103/PhysRevB.70.035211
16. Yeh CY, Lu ZW, Froyen S, Zunger A (1992) Zinc-blende–wurtzite polytypism in semiconductors. Phys Rev B 46:10086–10097
17. Ricolleau C, Audinet L, Gandais M, Gacoin T (1999) Structural transformations in II–VI semiconductor nanocrystals. Eur Phys J D 9:565–570
18. Banerjee R, Jayakrishnan R, Ayyub P (2000) Effect of the size-induced structural transformation on the band gap in CdS nanoparticles. J Phys Condens Matter 12:10647–10654. doi:10.1088/0953-8984/12/50/325
19. Xiong YS, Zhang J, Huang F, Ren GQ, Liu WZ, Li DS, Wang C, Lin Z (2008) Growth and phase transformation mechanisms of nanocrystalline CdS in Na_2S solution. J Phys Chem C 112:9229–9233. doi:10.1021/jp801628e
20. Suslick KS (ed) (1988) Ultrasound: its chemical, physical and biological effects. Wiley-VCH, Weinheim
21. Ashokkumar M (1998) An overview on semiconductor particulate systems for photoproduction of hydrogen. Int J Hydrog Energy 23:427–438
22. Henglein A (1982) Photochemistry of colloidal cadmium sulfide. 2. Effects of adsorbed methyl viologen and of colloidal platinum. J Phys Chem 86:2291–2293
23. Hong RY, Li JH, Chen LL, Liu DQ, Li HZ, Zheng Y, Ding J (2009) Synthesis, surface modification and photocatalytic property of ZnO nanoparticles. J Powder Technol 189:426–432. doi:10.1016/j.powtec.2008.07.004
24. Chandran Preethy, Pooja Kumari S, Khan Sudheer (2014) Photocatalytic activation of CdS NPs under visible light for environmental cleanup and disinfection. Sol Energy 105:542–547. doi:10.1016/j.solener.2014.04.028
25. Li Y, Li X, Li J, Yin J (2006) Photocatalytic degradation of methyl orange by TiO_2-coated activated carbon and kinetic study. Water Res 40:1119–1126. doi:10.1016/j.watres.2005.12.042
26. Wang P, Huang B, Qin X, Zhang X, Dai Y, Wei J, Whangbo MH (2008) Ag@ AgCl: a highly efficient and stable photocatalyst active under visible light. Angew Chem Int Ed 47:7931–7933. doi:10.1002/anie.200802483
27. Al-Qaradawi S, Salman SR (2002) Photocatalytic degradation of methyl orange as a model compound. J Photochem Photobiol A 148:161–168
28. Jian-Xi Y, Gao-Ling Z, Gao-Rong H (2003) The effect of the ratio of thiourea to Cd^{2+} on the properties of CdS nanoparticles. Microelectron Eng 66:115–120. doi:10.1016/S0167-9317(03)00034-0
29. Pattabi M, Saraswathi Amma B, Manzoor K (2007) Photoluminescence study of PVP capped CdS nanoparticles embedded in PVA matrix. Mater Res Bull 42:828–835. doi:10.1016/j.materresbull.2006.08.029
30. Moffitt M, Eisenberg A (1995) Size control of nanoparticles in semiconductor-polymer composites. 1. Control via multiplet aggregation numbers in styrene-based random ionomers. Chem Mater 7:1178–1184
31. He R, Qian XF, Yin J, Xi H, Bian L, Zhu ZK (2003) Formation of monodispersed PVP-capped ZnS and CdS nanocrystals under microwave irradiation. Colloids Surf A 220:151–157. doi:10.1016/S0927-7757(03)00072-4

32. Cullity BD, Stock SR (2001) Elements of X-ray diffraction, 3rd edn. Prentice Hall, New Jersey
33. Guo L, Yang S, Yang C, Yu P, Wang J, Ge W, Wong GKL (2000) Highly monodisperse polymer-capped ZnO nanoparticles: preparation and optical properties. Appl Phys Lett 76:2901–2903
34. Banerjee R, Jayakrishnan R, Ayyub P (2000) Effect of the size-induced structural transformation on the band gap in CdS nanoparticles. J Phys Condens Matter 12:10647. doi:10.1088/0953-8984/12/50/325
35. Muller RH, Jacobs C, Kayser O (2001) Nanosuspensions as particulate drug formulations in therapy rationale for development and what we can expect for the future. Adv Drug Deliv Rev 47:3–19
36. Pecora R (1985) Dynamic light scattering: application of photon correlation spectroscopy. Plenum Press, New York
37. Deonarine A, Hsu-Kim H (2009) Precipitation of mercuric sulfide nanoparticles in NOM-containing water: implications for the natural environment. Environ Sci Technol 43:2368–2373. doi:10.1021/es803130h
38. Xiang D, Zhu Y, Cai C, He Z, Liu Z, Yin D, Luo J (2011) A new simple synthesis of CdS nanoparticles by composite-molten-salt method and their high photocatalytic degradation activity. Phys E 44:733–737. doi:10.1016/j.physe.2011.11.023
39. Shi JW, Yan X, Cui HJ, Zong X, Fu ML, Chen S, Wang L (2012) Low-temperature synthesis of CdS/TiO_2 composite photocatalysts: influence of synthetic procedure on photocatalytic activity under visible light. J Mol Catal A Chem 356:53–60. doi:10.1016/j.molcata.2012.01.001
40. Guo X, Chen C, Song W, Wang X, Di W, Qin W (2014) CdS embedded TiO_2 hybrid nanospheres for visible light photocatalysis. J Mol Catal A Chem 387:1–6. doi:10.1016/j.molcata.2014.02.020
41. Zhang L, Sun F, Zuo Y, Fan C, Xu S, Yang S, Gu F (2014) Immobilisation of CdS nanoparticles on chitosan microspheres via a photochemical method with enhanced photocatalytic activity in the decolourisation of methyl orange. Appl Catal B 156–157:293–300. doi:10.1016/j.apcatb.2014.03.015
42. Al-Ekabi H, Serpone N (1988) Kinetic studies in heterogeneous photocatalysis. 1. Photocatalytic degradatlon of chlorinated phenols in aerated aqueous solutions over TiO_2 supported on a glass matrix. J Phys Chem 92:5726–5731
43. Smyth CP (1965) Dielectric behaviour and structure. McGraw-Hill, New York
44. Abdulkhadar M, Thomas B (1995) Study of dielectric properties of nano-particles of cadmium sulphide. Phys Stat Sol A 150:755–762. doi:10.1002/pssa.2211500219
45. Laha A, Krupanidhi SB (2003) Dielectric response and impedance spectroscopy of 0.7Pb (Mg 1/3 Nb 2/3) O 3–0.3 $PbTiO_3$ thin films. Mater Sci Eng B 98:204–212. doi:10.1016/S0921-5107(03)00033-3
46. Macdonald JR (1992) Impedance spectroscopy. Ann Biomed Eng 20:289–305